Carbohydrate Polymers 119 (2015) 26–34

Contents lists available at ScienceDirect

Carbohydrate Polymers

journal homepage: www.elsevier.com/locate/carbpol

β-Cyclodextrin polymer as a linker to fabricate ternary nanocomposites AuNPs/pATP-β-CDP/rGO and their electrochemical application

Ming Chen, Xiao Shen, Peipei Liu, Ying Wei, Yang Meng, Gang Zheng, Guowang Diao*

College of Chemistry and Chemical Engineering, Yangzhou University, Yangzhou 225002, PR China

ARTICLE INFO

Article history:
Received 1 July 2014
Received in revised form 3 November 2014
Accepted 3 November 2014
Available online 20 November 2014

Keywords:
β-Cyclodextrin polymer
Reduced graphene oxide
Gold nanoparticles
Imidacloprid
Oxygen reduction

ABSTRACT

Based on the self-assembly strategy, β-cyclodextrin polymer (β-CDP) was used as a linker to connect reduced graphene oxide (rGO) and *p*-aminothiophenol (pATP). Then, pre-prepared gold nanoparticles (AuNPs) can self-assemble onto the surface of pATP-β-CDP/rGO to obtain new ternary nanocomposites AuNPs/pATP-β-CDP/rGO. The amount or the density of AuNPs can be adjusted by changing the concentration of pATP. UV–vis and ^{1}H NMR spectra confirmed the formation of inclusion complex between pATP and β-CDP. β-CDP might improve the dispersity of rGO in aqueous and the surface property of rGO. AuNPs/pATP-β-CDP/rGO modified electrode displayed high electrochemical response toward a pesticide-imidacloprid (IDP). The enrichment capability and molecular recognition of β-CDP and the catalytic property of AuNPs for IDP molecules synergistically promoted the electrochemical response of rGO modified electrode. Additionally, ternary nanocomposites exhibited the good electrocatalytic performance for oxygen reduction in O_2-saturated 0.1 M H_2SO_4 solution. The proposed synthesis strategy provided a facile, feasible and effective method for development of electrochemical sensors and Au-based catalysts for fuel cells.

1. Introduction

Recently, graphene nanosheet (GN) has attracted considerable attention due to its extraordinary electronic, thermal, mechanical and chemical properties (Balandin, 2011; Castro Neto, Guinea, Peres, Novoselov, & Geim, 2009; Geim, 2009; Zhu et al., 2010). The integration of GN and metal/metal oxide as new generation hybrid materials has the potential to construct various applied platforms such as catalysis (Kou et al., 2011), electrochemical sensor (Shao et al., 2010), and electrochemical energy storage (Wang et al., 2009). So far, metal nanoparticles/GN hybrid materials have been fabricated through two different methods, including in situ growth method (Wang et al., 2011) and self-assembly method (Hong et al., 2010; Ren, Fang, & Wang, 2011). Self-assembly metal nanoparticles on GN using the intermedia is an important strategy for fabricating metal-GN composites, where certain linkers, such as poly(diallyldimethyl ammonium chloride) (Ren et al., 2011), 1-pyrene butyric acid (Hong et al., 2010), DNA (Liu, Choi, & Seo, 2010a), protein (Liu, Fu, Yuan, Li, & Deng, 2010b), and calixarene (Zhou, Chen, & Diao, 2013a; Zhou, Chen, Xie, & Diao, 2013b) can bind metallic nanoparticles to GN planes. Furthermore, self-assembly method is a moderate approach, which might efficiently control the dispersion and adjust the loading amount of nanoparticles with varying sizes, shapes and types on the surface of GN (Liu et al., 2010b; Zhou et al., 2013a).

β-Cyclodextrin (β-CD) is cyclic oligosaccharides including glucose unites linked by α-1,4-glucosidic bonds. β-CD can capture various inorganic and organic molecules into its cavity to form host-guest inclusion complexes (Chen, Diao, & Zhang, 2006; Mamba, Mbianda, & Govender, 2013; Badruddoza, Shawon, Tay, Hidajat, & Uddin, 2013), owing to its hydrophobic internal cavity and hydrophilic external surface. β-Cyclodextrin/graphene hybrid nanosheets as ideal building blocks in nanocomposites have been prepared (Guo et al., 2010; Konkena & Vasudevan, 2013; Ogoshi, Ichihara, Yamagishi, & Nakamoto, 2010; Zu & Han, 2009), and extensively applied in electrochemical sensors and biosensors due to the special recognition and enrichment functions of β-CD (Dong et al., 2013; Guo, Guo, Li, Wang, & Dong, 2011; Lu et al., 2012; Lv et al., 2013; Tan et al., 2010; Yang et al., 2012; Zhang, Gu, Ding, Shen, & Jiang, 2014). However, low solubility (18.5 g L^{-1}, 25 °C) and week recognition capacity of β-CD restrict the application to improve the solubility and stability of functional materials. β-cyclodextrin polymer (β-CDP) has better solubility in water (>100 g L^{-1}, 25 °C) and stronger molecule recognition ability than β-CD (Chen et al.,

* Corresponding author. Tel.: +86 514 87975436; fax: +86 514 87975244.
E-mail address: gwdiao@yzu.edu.cn (G. Diao).

http://dx.doi.org/10.1016/j.carbpol.2014.11.022
0144-8617/

2013a; Chen, Wang, Zhang, & Diao, 2013b; Zhang, Chen, & Diao, 2011). Our research group firstly synthesized β-CDP/rGO composite, which displayed the excellent water-dispersity, and stability, and exhibited the high supramolecular recognition and enrichment capability for guest molecules, such as ferrocenemethanol, hypericin, pesticide-imidacloprid (IDP) (Zhang, Chen, Gong, & Diao, 2013; Zhang et al., 2013b; Chen et al., 2013a).

In view of the excellent performances of rGO/β-CDP and metal nanoparticles, respectively, they are effectively integrated into a new ternary composite. New ternary nanocomposites might possess three materials individual properties, such as large surface area and high conductivity of rGO, supramolecular recognition and enrichment capability of β-CDP and catalytic property of metal nanoparticles. The integration of rGO, β-CDP and metal nanoparticles will expand potential applications in various fields such as sensors, electrocatalysis and biological probe, and thus arouse extensive research interest.

In this study, based on the self-assembly strategy, β-CDP was used as a linker to connect rGO and *p*-aminothiophenol (pATP). Then, pre-prepared AuNPs can self-assemble onto the surface of pATP-β-CDP/rGO through thiol and amido groups of pATP to obtain new ternary nanocomposites AuNPs/pATP-β-CDP/rGO. Lastly, we have explored the electrochemical property of AuNPs/pATP-β-CDP/rGO. Ternary nanocomposites show good electrochemical response toward imidacloprid and high catalytic property for oxygen reduction reaction.

2. Experimental

2.1. Materials

Natural graphite powder (99.99%) was obtained from Sigma-Aldrich (USA). β-Cyclodextrin (β-CD), *p*-aminothiophenol (pATP), hydrazine hydrate, $HAuCl_4{\cdot}3H_2O$ powder, imidacloprid (IDP), and sodium borohydride ($NaBH_4$) were purchased from Sinopharm Chemical Reagents Company. Other chemicals and solvents are reagent grade and commercially available. Deionized water was used to prepare all solution.

2.2. Characterization

Ultraviolet–visible (UV–vis) absorption spectra were measured on a UV-2550 PC UV–visible spectrometer (Shimadzu, Japan). The ^{1}H NMR spectra were conducted on a 600 MHz Bruker spectrometer (Bruker, Germany) at 303.1 K in D_2O. Contact angles were measured on a drop shape analysis system Dataphysics/OCA40 (Germany) contact angle system. Diffraction (XRD) data were obtained with a graphite monochromator and Cu $K\alpha$ radiation ($\lambda = 0.1541$ nm) on a D8 advance superspeed powder diffractometer (Bruker). TEM (Transmission Electron Microscopy) observation was conducted on a Philips TECNAI-12 instrument. The Energy-dispersive X-ray (EDX) analysis was performed on a KEVEX X-ray energy detector. Electrochemical impedance spectroscopy (EIS) was measured with an Autolab/PG30 electrochemical analyzer system (ECO Chemie B. V. Netherlands).

All electrochemical experiments were operated with a CHI660c electrochemical workstation (Chenghua, China) with a three-electrode system including a glass carbon electrode (GCE) ($d = 3$ mm) as the working electrode, a Pt wire electrode as the counter electrode, a saturated calomel electrode (SCE) as the reference electrode. AuNPs/pATP-β-CDP/rGO, pATP-β-CDP/rGO, β-CDP/rGO and rGO were dispersed in deionized water to prepare the suspensions (0.5 mg mL^{-1}). The suspensions (10 μL) were spread on the surface of glass carbon disk electrodes. The coating was dried in air at room temperature to obtain the modified electrode.

2.3. Preparation of AuNPs/pATP-β-CDP/rGO ternary nanocomposites

β-CDP was synthesized by cross-linking β-CD with EP under a strongly alkaline condition (33 wt% NaOH). The molar ratio of β-CD/epichlorohydrin was 1:7. The details of the synthesis and purification were shown as in the reference (Zhang, Chen, & Diao, 2011). The preparation of AuNPs/pATP-β-CDP/rGO with different AuNPs loading amount is shown in Scheme 1. First, water-soluble β-CDP are modified on GO according to previously reported methods (Chen et al., 2013b). GO was synthesized from natural graphite powder by Hummer's method (Hummers and Offeman, 1958). β-CDP was synthesized following previously reported methods (Zhang et al., 2011). Then, as shown in Scheme 1b and b', in a typical procedure, β-CDP/GO (0.2 g) was dispersed in different concentration of pATP ethanol solution (10 ml) by bath-sonicating and then the mixtures were allowed to stir for 12 h at room temperature. In Scheme 1c and c', after adding hydrazine hydrate (100 μL) and ammonia solution (200 μL), mixtures were stirred vigorously at 80 °C for 12 h. The stable black dispersion was separated by centrifuging and washed with doubly distilled water three times to obtain pATP-β-CDP/rGO. Lastly, a colloid solution of AuNPs (an

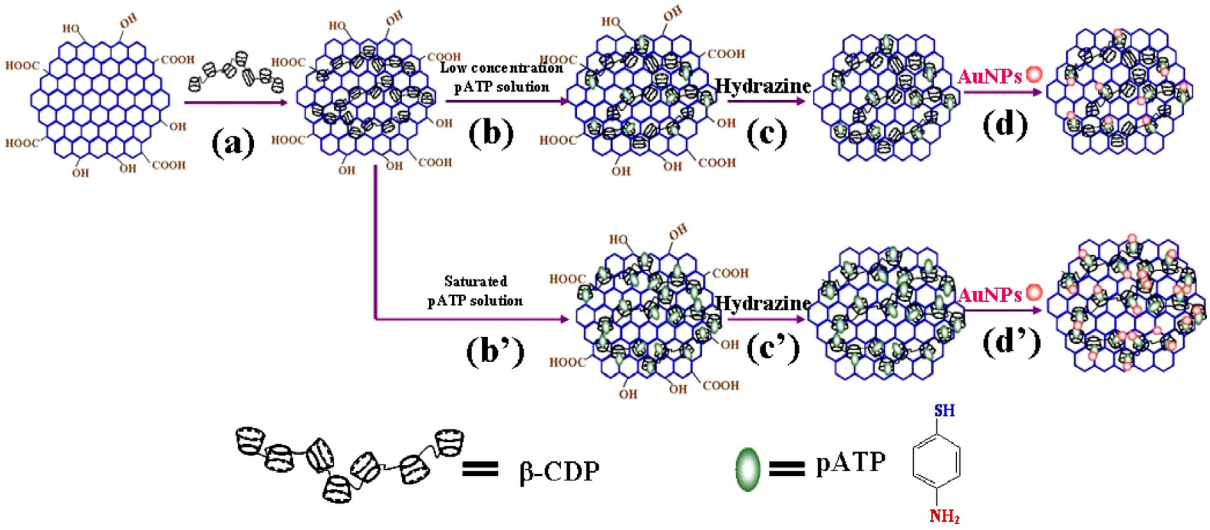

Scheme 1. Schematic diagram of the procedure for preparing AuNPs/pATP-β-CDP/rGO with different AuNPs loading amount.

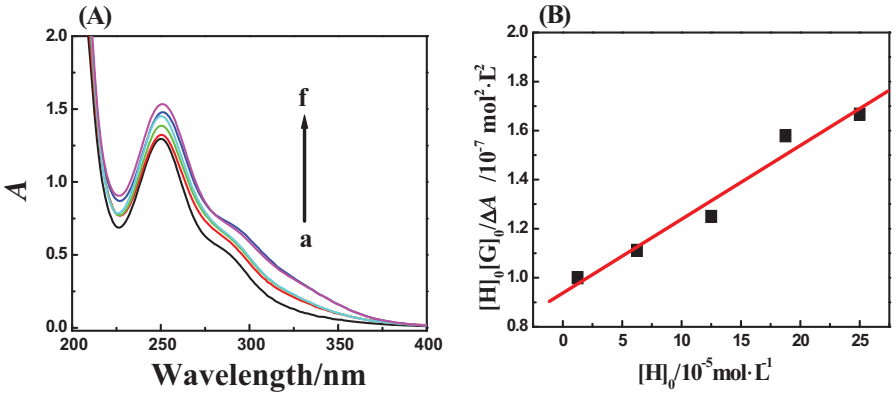

Fig. 1. (A) At 25 °C, UV–vis spectra of 1.6×10^{-4} mol L^{-1} pATP aqueous solution with different concentrations of β-CDP (10^{-5} mol L^{-1}): (a) 0, (b) 1.25, (c) 6.25, (d) 12.5, (e) 18.7, (f) 25.0. (B) The plot of $[H]_0[G]_0/\Delta A$ vs. $[H]_0$.

average diameter 5 nm) was prepared according to the literature reported by Grabar (Grabar et al., 1996). Pre-synthesized AuNPs self-assemble onto pATP-β-CDP/rGO to synthesize AuNPs/pATP-β-CDP/rGO nanocomposites. pATP-β-CDP/rGO (20 mg) was added to the excess as-prepared AuNPs under vigorous stirring and these mixtures were ultrasonicated for 3 min (Scheme 1d and d'). After stirring for an additional 1 h, black solids were separated by centrifugation and washed with deionized water for three times, and then dried 24 h in a vacuum drying oven at 60 °C.

3. Results and discussion

3.1. Characterization of pATP-β-CDP

The dissociated constant of the inclusion compound between pATP and β-CDP can be determined by UV–vis spectroscopy. In neutral solution (pH = 7.0), the UV–vis spectra at a given concentration of pATP with different concentrations of β-CDP were shown in Fig. 1A. The peak position is independent of the concentrations of β-CDP. However, the peak intensity increases with the concentrations of β-CDP, which indicates that the molar absorption coefficient of the inclusion complex is larger than that of pATP itself. As previously described (Chen et al., 2006), if one makes assumptions of 1:1 ratio of pATP to β-CD units of β-CDP in inclusion compound, the relationship of the peak intensity and the concentration of β-CDP can be deduced as the following equation:

$$\frac{[H]_0[G]_0}{\Delta A} = \frac{[H]_0}{\Delta \varepsilon} + \frac{K_D}{\Delta \varepsilon} \quad (1)$$

where $[H]_0$ and $[G]_0$ are the initial concentrations of β-CDP and pATP, respectively, ΔA is the difference of peak intensity of pATP with and without β-CDP, $\Delta \varepsilon$ is the difference of molar absorption coefficient between inclusion compound and pATP, K_D is the dissociated constant of the inclusion compound. According to Eq. (1), the plot of $[H]_0[G]_0/\Delta A$ versus $[H]_0$ should be a straight line. The experimental result was shown in Fig. 1B. A well behaved linear relationship between $[H]_0[G]_0/\Delta A$ and $[H]_0$ shows that the assumption of 1:1 ratio of pATP to β-CD units of β-CDP in inclusion compound is correct. From the slope and the intercept of the line, the dissociated constant, K_D is evaluated as 3.2×10^{-6} mol L^{-1}. According to the same method, the dissociated constant of the inclusion complex with the stoichiometric ratio 1:1 between β-CD and pATP is evaluated as 7.4×10^{-2} mol L^{-1}, which is far larger than that between β-CDP and pATP, confirming the higher stability of inclusion complex of pATP-β-CDP.

Fig. 2 shows the typical ^{1}H NMR spectra of (a) pATP, (b) β-CDP, and (c) pATP-β-CDP in D_2O. The chemical structure and the hydrogen atom of pATP and β-CD unit in β-CDP are listed in Fig. 2(a) and (b). In Fig. 2(a), Ha and Hb protons of benzene ring appear at 6.686 and 7.117 ppm, respectively. Active hydrogen atoms (—SH and —NH_2) were replaced by D_2O, so they did not show the corresponding chemical shift. In Fig. 2(b), the H1 of β-CD unit appears at 4.97 ppm, well apart from the rest of the signals. The H2-H6a,b of β-CD unit and hydroxypropyl ether unit appear in the same region from 3.20 to 4.30 ppm, forming several broad peaks in Fig. 2(b). The ^{1}H NMR spectrum of complex inclusion of pATP-β-CDP is shown in Fig. 2(c). The proton peaks of guest and host molecule appear simultaneously, which implies that pATP reacts with β-CDP to form inclusion complex. The chemical shifts of Ha and Hb of pATP are moved to 6.626 and 7.102 ppm, respectively. More interesting, two new peaks appear at 2.727 and 2.886 ppm, respectively, which are assigned to active hydrogen atoms (—SH and —NH_2). Because the pATP monomer enters into the hydrophobic cavity of β-CD, active hydrogen atoms (—SH and —NH_2) cannot be completely replaced by D_2O, causing the appearance of peaks of active hydrogen atoms. Therefore, the results of ^{1}H NMR spectra indicate that the pATP guest penetrates into β-CD cavity of β-CD polymer to form inclusion complex.

3.2. Dispersity and hydrophily of β-CDP/rGO

Due to the prominent interlayer π–π stacking interaction of rGO, it is inclined to aggregate and eventually precipitate. In Fig. 3A(a), rGO is almost not dispersive in water. However, β-CDP might increase the dispersity of rGO in aqueous. With the increase of the quality of β-CDP, the dispersity of rGO in water was increased (Fig. 3A(b)–(d)). Even if rGO (2 mg) in β-CDP solution (4 mg mL^{-1}) was stored two months, no precipitation was formed. The excellent dispersity of β-CDP/rGO composite is attributed to the strong adhesive force of β-CDP on rGO and high solubility of β-CDP in water.

Additionally, the surface properties of rGO and β-CDP/rGO were further characterized by static contact angles to investigate their hydrophilic/hydrophobic features. In Fig. 3B(a), the contact angle for water on rGO film was measured to be 112°, which confirms that rGO has a hydrophobic interface. In contrast, β-CDP/rGO films are comparatively more hydrophilic, indicating that the surface of rGO was decorated by water-soluble β-CDP molecule. With the increase of the quality of β-CDP, the contact angles were decreased (Fig. 3B(b)–(d)), which demonstrates that the more β-CDP are loaded on rGO, the stronger the hydrophily of β-CDP/rGO films have.

3.3. Characterization of AuNPs/pATP-β-CDP/rGO ternary nanocomposites

The successful synthesis of pATP-β-CDP/rGO and AuNPs/pATP-β-CDP/rGO are confirmed by UV–vis absorption spectra. As shown

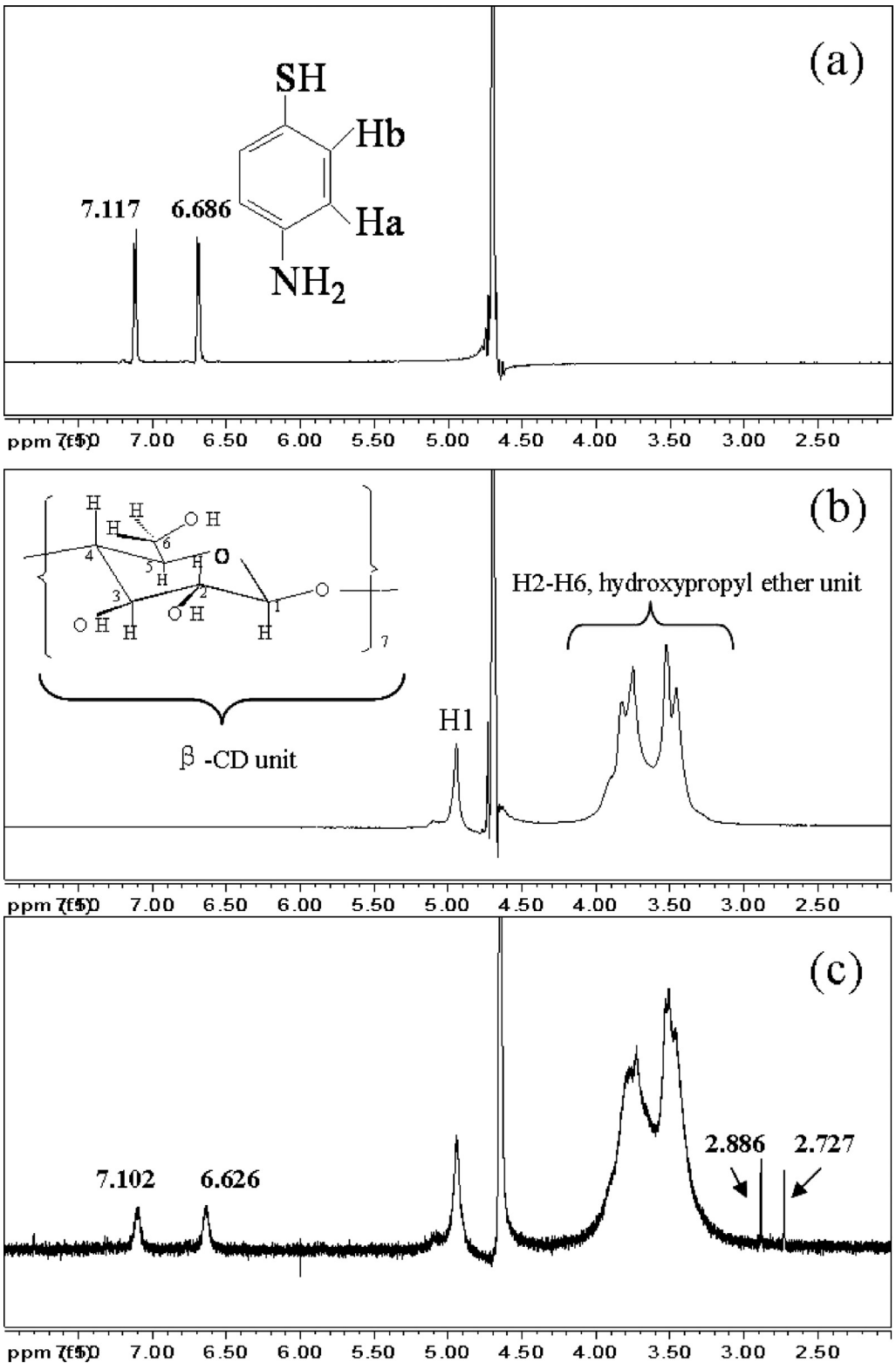

Fig. 2. ^{1}H NMR spectra of (a) pATP, (b) β-CDP, (c) pATP-β-CDP.

in Fig. 4a, the characteristic absorption peak of pATP is at 251 nm, corresponding to $\pi \rightarrow \pi^*$ electron transition of benzene ring. β-CDP has no UV–vis absorption, so a broad peak of β-CDP/rGO is at about 270 nm, which is attributed to UV–vis absorption of rGO (Fig. 4b). In Fig. 4c, the peak at 251 nm in pATP-β-CDP/rGO is assigned to the absorbance peak of pATP, confirming the attachment of pATP on the surface of rGO through the formation of inclusion complex. The characteristic absorption peak of AuNPs shows at 522 nm (Fig. 4d). When AuNPs self-assembled on the surface of pATP-β-CDP/rGO through thiol and amino groups of pATP, two main absorption peaks appear at the UV–vis spectrum of AuNPs/pATP-β-CDP/rGO (Fig. 4e), which indicates that AuNPs are modified on β-CDP-pATP/rGO. The self-assembly process results in the red shift of the surface plasma resonance of AuNPs. Simultaneously,

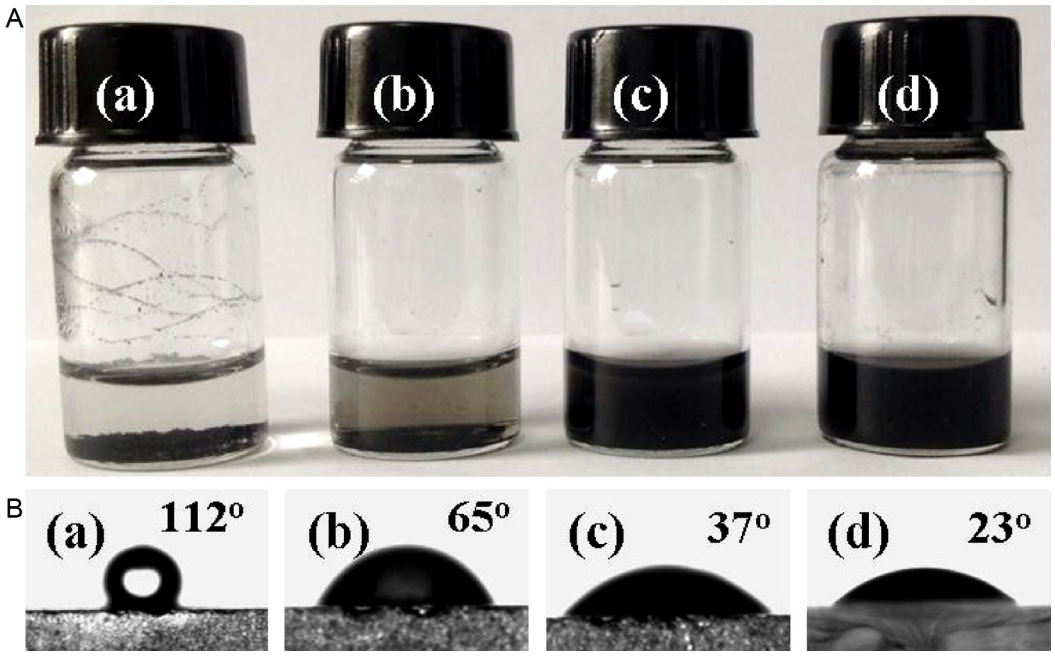

Fig. 3. (A) Photos of 2 mg rGO dispersions in aqueous media with different concentrations of β-CDP/(mg mL^{-1}): (a) 0, (b) 1, (c) 2, (d) 4. (B) Static contact angles of (a) rGO, (b–d) β-CDP/rGO corresponding to the products obtained from A(b–d).

the coordination between thiol/amino groups of pATP and AuNPs decreases the system energy, leading to the red shift (from 251 nm to 263 nm) of pATP absorption peak. Therefore, UV–vis absorption spectra confirm the successful preparation pATP-β-CDP/rGO and AuNPs/pATP-β-CDP/rGO.

Fig. 5 shows XRD patterns of (a) rGO, (b) β-CDP, (c) β-CDP/rGO, (d) pATP-β-CDP/rGO and (e) AuNPs/pATP-β-CDP/rGO. A broad peak at 23.9° is assigned to the feature peak of rGO (Fig. 5a). β-CDP shows a representative noncrystal diffraction peak at 18.7° (Fig. 5b). When β-CDP was adsorbed on rGO, the peak at 19.5° might be the overlay peaks of β-CDP and rGO (Fig. 5c). In Fig. 5d, XRD pattern of pATP-β-CDP/rGO is similar to β-CDP/rGO. In Fig. 5e, the peaks at $2\theta = 38.4°$, 44.4°, 64.8°, and 77.9° are attributed to the Au (1 1 1), (2 0 0), (2 2 0) and (3 1 1), respectively, which demonstrates the successful fabrication of AuNPs/pATP-β-CDP/rGO nanocomposites.

TEM images show that AuNPs self-assemble onto rGO to form AuNPs/pATP-β-CDP/rGO composites by using pATP-β-CDP as a medium. Fig. 6 shows the TEM images of AuNPs/pATP-β-CDP/rGO composites prepared with different concentrations of pATP. The homogeneous AuNPs with average diameter 5 nm are well dispersed on rGO through the connection of pATP-β-CDP. Apparently, with the increase of concentrations of pATP, the density of AuNPs on pATP-β-CDP/rGO is increased. Depending on bifunctional compound pATP-β-CDP, this strategy is also appropriate for modifying other noble metals nanoparticles on the surface of rGO to fabricate noble metal nanoparticles/pATP-β-CDP/rGO ternary nanocomposites, such as Ag, Pt (see Supplementary data).

To confirm AuNPs adsorbed on the surface of pATP-β-CDP/rGO and obtain the content of AuNPs in the composites, AuNPs/pATP-β-CDP/rGO composites were characterized by EDX. Fig. 7 is representative EDX spectrum of AuNPs/pATP-β-CDP/rGO synthesized at pATP 1×10^{-3} mol L^{-1}. EDX spectrum displays that the main elemental compositions of the nanocomposites are Au, C, N, O and S. The result indicates that AuNPs are well-absorbed onto the surface of rGO through the link of pATP-β-CDP. The element Na comes from trisodium citrate, which is adsorbed on the surface of AuNPs to form the electric double layer. Furthermore, the contents of AuNPs in the composites are increased with the increase of the concentrations of pATP. The contents of AuNPs in the composites are 2.6%, 6.7%, 15.7%, and 23.2%, corresponding 1×10^{-4}, 5×10^{-4}, 1×10^{-3} mol L^{-1}, and saturation solution of pATP (1.2×10^{-3} mol L^{-1}), respectively. The high loading amount of AuNPs on pATP-β-CDP/rGO might ascribe to the strong interaction

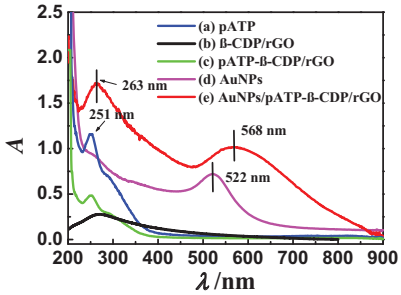

Fig. 4. UV–vis spectra of (a) pATP, (b) β-CDP/rGO, (c) pATP-β-CDP/rGO, (d) AuNPs, (e) AuNPs/pATP-β-CDP/rGO.

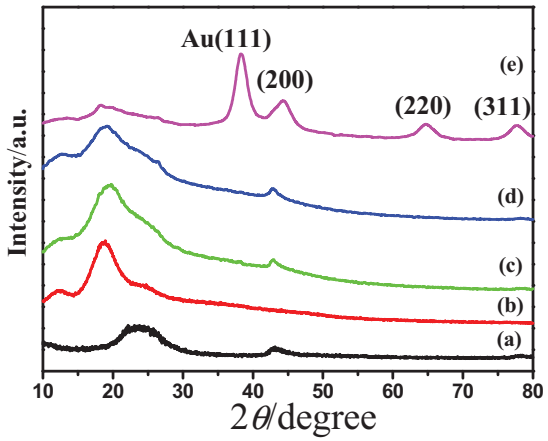

Fig. 5. XRD patterns of (a) rGO, (b) β-CDP, (c) β-CDP/rGO, (d) pATP-β-CDP/rGO, (e) AuNPs/pATP-β-CDP/rGO.

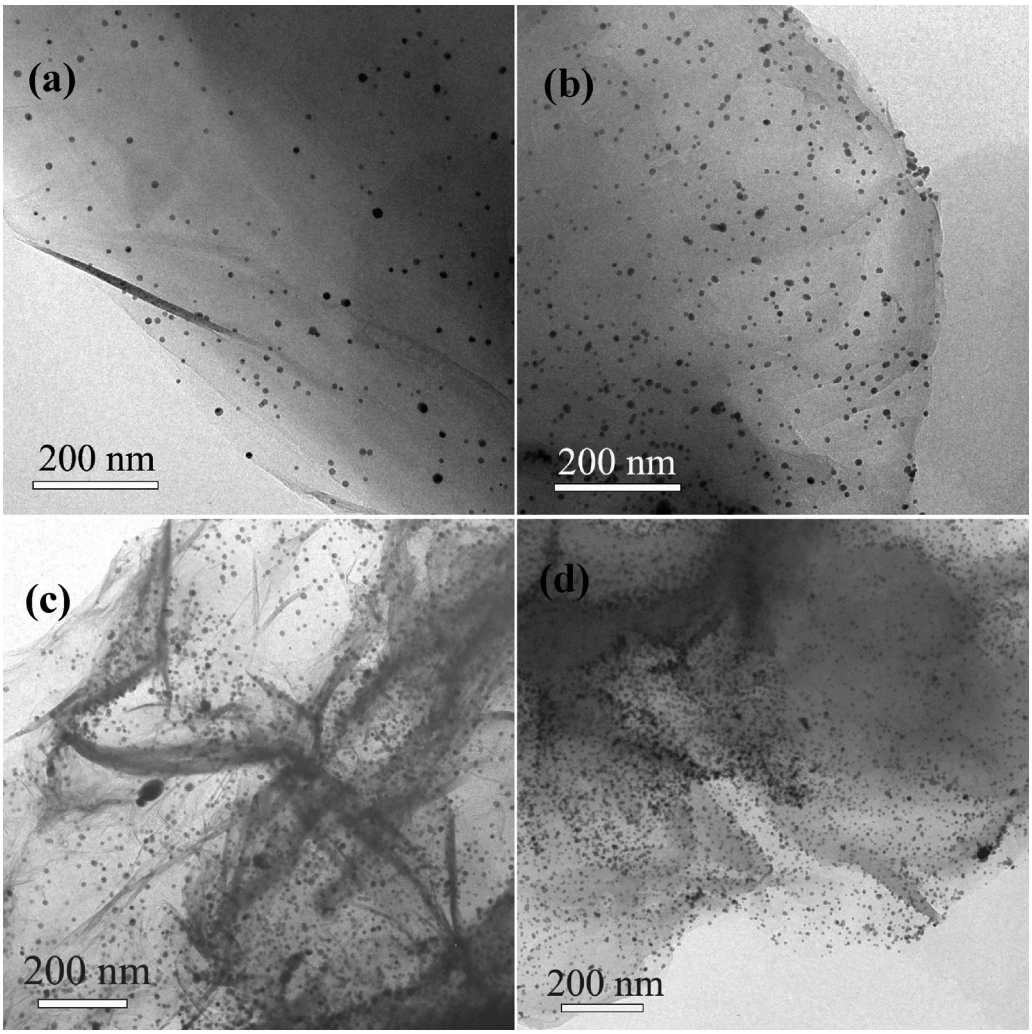

Fig. 6. TEM images of AuNPs/pATP-β-CDP/rGO obtained at different concentrations of pATP. Concentrations of pATP/mol L^{-1}: (a) 1×10^{-4}, (b) 5×10^{-4}, (c) 1×10^{-3}, (d) saturation solution (1.2×10^{-3} mol L^{-1}).

between AuNPs and–SH/–NH_2 groups of pATP (Yee et al., 1999; Cui et al., 2011; Shen, Du, Rong, Li, & Jiang, 2005).

3.4. Electrocatalytic reduction of IDP on AuNPs/pATP-β-CDP/rGO/GCE electrode

Ternary nanocomposites AuNPs/pATP-β-CDP/rGO can exhibit multifunctional properties, such as large surface area and excellent electronic transfer of rGO, molecular recognition and enrichment performances of β-CDP, and good catalytic property and biocompatibility of AuNPs. According to previous work of our group, β-CDP/rGO/GCE exhibited an excellent electrochemical performance for IDP (Chen et al., 2013a). Because β-CDP can trap with IDP to form an inclusion complex, the interaction between β-CDP and IDP can enhance the accumulation effects of β-CDP/rGO/GCE and accordingly increase the peak current related to both bare GCE and rGO/GCE electrodes. While AuNPs self-assemble on pATP-β-CDP/rGO, ternary nanocomposites AuNPs/pATP-β-CDP/rGO might perform the synergetic action of multifunctional properties.

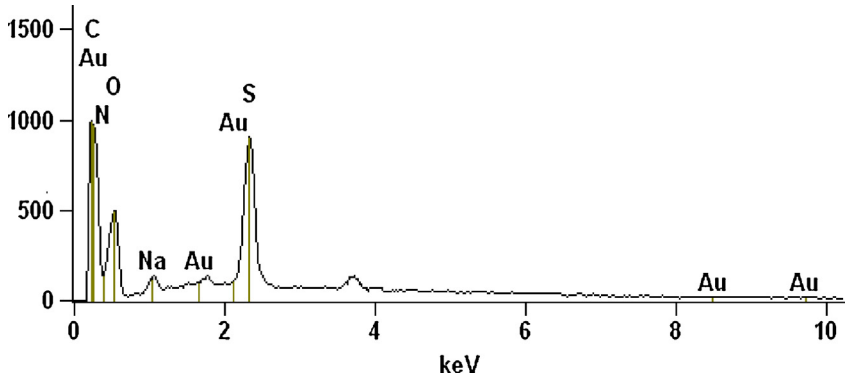

Fig. 7. EDX spectrum of AuNPs/pATP-β-CDP/rGO synthesized at pATP 1×10^{-3} mol L^{-1}.

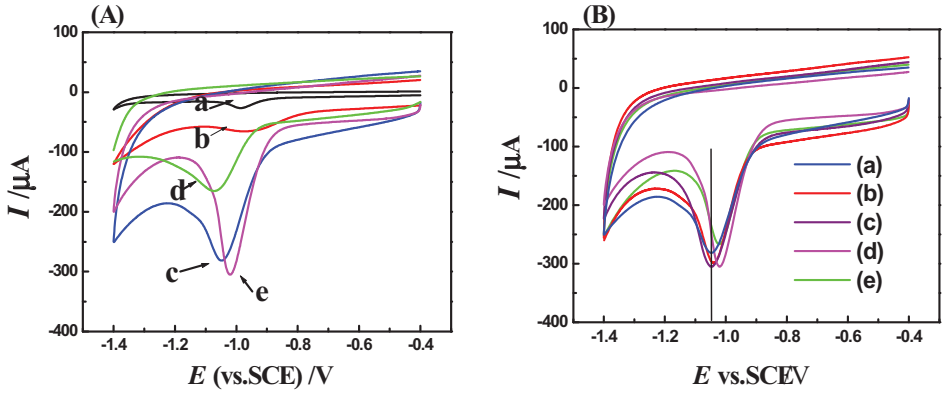

Fig. 8. (A) Cyclic voltammograms at a scan rate of 0.1 V s^{-1} for (a) bare GCE, (b) rGO/GCE, (c) β-CDP/rGO/GCE, (d) pATP-β-CDP/rGO/GCE, (e) AuNPs/pATP-β-CDP/rGO/GCE in 1×10^{-4} mol L^{-1} IDP solution and 0.2 mol L^{-1} phosphate buffer solution. (B) Cyclic voltammograms at a scan rate of 0.1 V s^{-1} for AuNPs/pATP-β-CDP/rGO/GCE obtained with different concentrations of pATP in 1×10^{-4} mol L^{-1} IDP solution and 0.2 mol L^{-1} phosphate buffer solution. (a) β-CDP/rGO/GCE. Concentrations of pATP/mol L^{-1}: (b) 1×10^{-4}, (c) 5×10^{-4}, (d) 1×10^{-3}, (e) saturation solution.

In order to confirm above hypothesis, IDP is chosen as a guest molecule and the electrochemical behaviors of IDP were investigated on different modified electrodes. Cyclic voltammograms (CVs) of 1×10^{-4} mol L^{-1} IDP on different modified electrodes are shown in Fig. 8A. In curve a, a weak reduction peak is ascribed to the electrochemical reduction of nitric group,–NO_2 in IDP on the bare GCE. In curve b, the peak current of IDP on rGO/GCE is larger than that on the bare GCE owing to the good conductivity and large surface area of rGO. Due to the accumulation effects of β-CDP, the peak current of IDP on β-CDP/rGO/GCE continues to increase (curve c). However, the peak current of IDP on pATP-β-CDP/rGO/GCE decreases corresponding to that on β-CDP/rGO/GCE (curve d). On account of the formation of inclusion complex between β-CDP and pATP, some cavities of β-CDP are occupied by pATP, resulting in the decline of accumulation effects of β-CDP. But, as AuNPs self-assemble on pATP-β-CDP/rGO, AuNPs will catalyze the electrochemical reduction of nitric group (Jiao, Luo, & Li, 2013; Liu, Zhang, Ma, & Hou, 2011; Silva, Gasparini, Magosso, & Spinelli, 2014; Tang et al., 2013). In curve e, the largest peak current of IDP was detected on AuNPs/pATP-β-CDP/rGO/GCE. Although pATP molecules occupy some cavities of β-CDP, the response current further achieves promotion owing to excellent catalytic property of AuNPs, which makes up for the weakening of accumulation effect of β-CDP. Schematic diagrams of the electrochemistry response on different modified electrodes are shown Scheme 2. rGO modified electrode shows low current (Scheme 2a). Binary composite β-CDP/rGO modified electrode achieves medium current (Scheme 2b). In Scheme 2c, the synergetic effect of ternary nanocomposites promotes electrochemical performance of modified electrode. It displays high electrochemistry response.

Fig. 8B shows that the AuNPs/pATP-β-CDP/rGO obtained at different concentration of pATP are used to catalyze the IDP reduction. It is found that AuNPs/pATP-β-CDP/rGO synthesized with 1×10^{-3} mol L^{-1} pATP displays the highest peak current. However, AuNPs/pATP-β-CDP/rGO obtained at saturation solution of pATP shows the smallest current for IDP reduction. Although ternary nanocomposites obtain the largest loading amount of AuNPs at saturation solution of pATP, all of cavities of β-CDP were occupied by pATP molecules, which leads to β-CDP lose the accumulation effect completely and accordingly the peak current decreases related to other ternary nanocomposites synthesized at low concentrations of pATP.

3.5. *Electrocatalytic oxygen reduction on AuNPs/pATP-β-CDP/rGO/GCE electrode*

As is well known, the large over-potential associated with oxygen reduction reaction is one of the major challenges that need the development of a high performance cathode catalyst. Here, the electrocatalytic activity of AuNPs/pATP-β-CDP/rGO has been investigated for oxygen reduction. Fig. 9A shows CVs of O_2 reduction on AuNPs/pATP-β-CDP/rGO/GCE in 0.1 M H_2SO_4

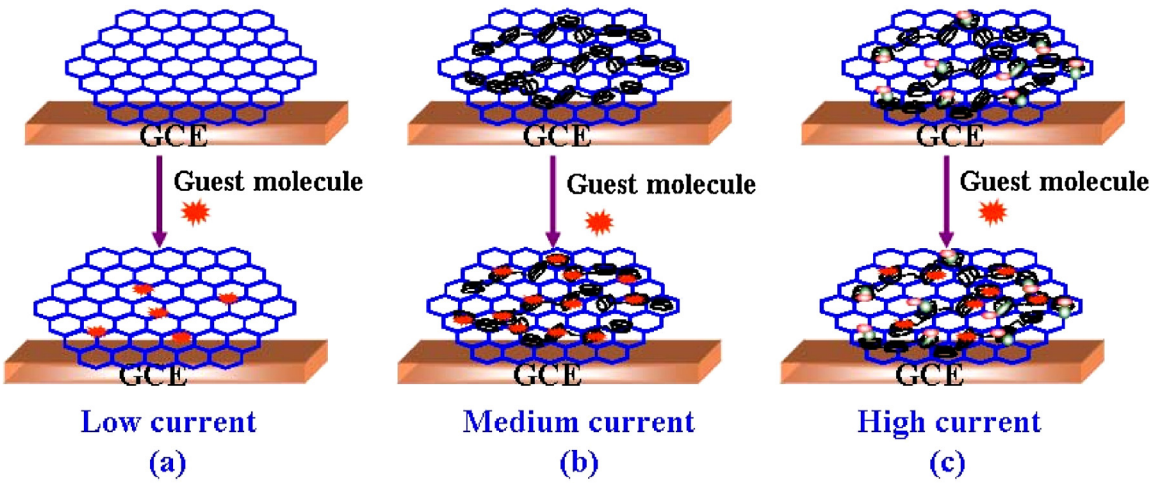

Scheme 2. Schematic diagram of electrochemistry response on different modified electrodes (a) rGO/GCE, (b) β-CDP/rGO/GCE, (c) AuNPs/pATP-β-CDP/rGO/GCE.

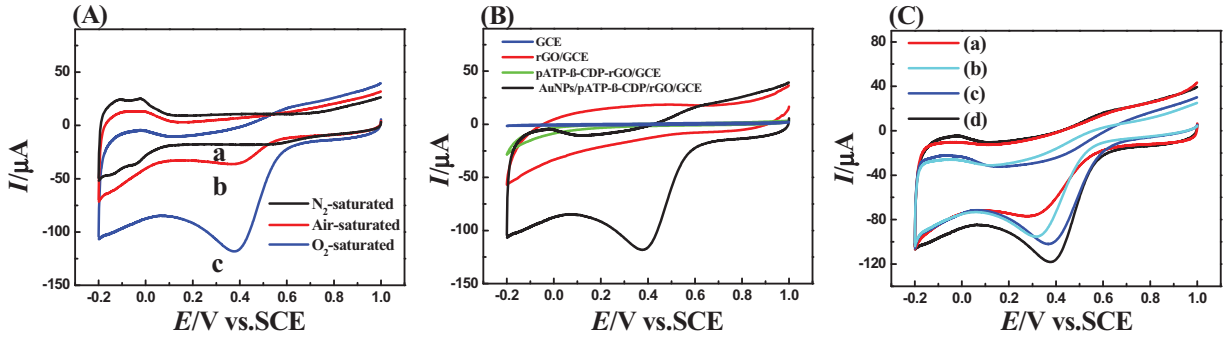

Fig. 9. (A) CVs of O_2 on the AuNPs/pATP-β-CDP/rGO synthesized at saturation pATP solution in (a) N_2-saturated, (b) air-saturated, (c) O_2-saturated 0.1 M H_2SO_4 solutions. (B) CVs of O_2 on different modified electrodes in O_2-saturated 0.1 M H_2SO_4 solutions. (C) CVs of O_2 on AuNPs/pATP-β-CDP/rGO obtained at different concentrations of pATP in O_2-saturated 0.1 M H_2SO_4 solutions. Concentrations of pATP/mol L^{-1}:(a) 1×10^{-4}, (b) 5×10^{-4}, (c) 1×10^{-3}, (d) saturation solution.

solution with saturated N_2 (curve a), saturated air (curve b) and saturated O_2 (curve c), respectively. No reduction current can be observed in the electrolyte solution with saturated N_2 (curve a), and a small reduction peak appears in the electrolyte solution with saturated air (curve b). However, when the electrolyte solution is saturated with O_2, the reduction peak current markedly increases (curve c), which indicates that AuNPs/pATP-β-CDP/rGO has good electrocatalytic activity for oxygen reduction.

Fig. 9B shows the CVs of O_2 reduction on different modified electrodes. Distinctly, bare GCE, rGO/GCE and pATP-β-CDP/rGO/GCE have no the electrocatalytic activity for oxygen reduction. Fig. 9C displays the CVs of O_2 reduction on AuNPs/pATP-β-CDP/rGO with different AuNPs loading amount. The electrocatalytic activity of AuNPs/pATP-β-CDP/rGO for oxygen reduction is adjustable by changing the loading amount of AuNPs on the rGO. With the increase of the amount of AuNPs, the catalytic currents increase gradually (Fig. 9C). The peak potentials show a positive shift from 0.30 V to 0.38 V, indicating that the larger loading amount of AuNPs might decrease reduction potentials and enhances the catalytic activity for oxygen reduction reaction.

4. Conclusions

In conclusion, we synthesized new ternary nanocomposites-AuNPs/pATP-β-CDP/rGO by self-assembly strategy. β-CDP was applied as a linker to connect rGO and pATP. UV–vis and ^{1}H NMR spectra confirmed the formation of inclusion complex between β-CDP and pATP. The dissociated constant, K_D is evaluated as 3.2×10^{-6} mol L^{-1}. The stability of inclusion complex between β-CDP and pATP is higher than inclusion complex between β-CD and pATP. β-CDP might enhance the dispersity of rGO in aqueous and transform the surface property of rGO from hydrophobicity to hydrophily. Then, pre-prepared AuNPs can self-assemble onto the surface of pATP-β-CDP/rGO to obtain ternary nanocomposites. The loading amount of AuNPs on rGO can be tunable by changing the concentration of pATP. AuNPs/pATP-β-CDP/rGO composites display high electrochemical response toward imidacloprid and good catalytic property for oxygen reduction reaction. The proposed synthesis method describes a moderate, elastic and effective process for the progress of electrochemical sensor and Au-based catalysts for oxygen reduction reaction.

Acknowledgements

This work was financially supported by the National Natural Science Foundation of China (Grant no. 21273195), cooperation fund from Yangzhou Government and Yangzhou University (Grant no. 2012038-9) and a Project Funded by the Priority Academic Program Development of Jiangsu Higher Education Institutions. The work was also sponsored by Qing Lan Project of Higher Learning Institutions in Jiangsu Province and Jiangsu Key Laboratory of Environmental Material and Environmental Engineering (K11032, K13062). The authors also acknowledge the Testing Center of Yangzhou University for ^{1}H NMR, TEM, XRD and EDX experiments.

Appendix A. Supplementary data

Supplementary data associated with this article can be found, in the online version, at http://dx.doi.org/10.1016/j.carbpol.2014.11.022.

References

Badruddoza, A. Z. M., Shawon, Z. B. Z., Tay, W. J. D., Hidajat, K., & Uddin, M. S. (2013). Fe_3O_4/cyclodextrin polymer nanocomposites for selective heavy metals removal from industrial wastewater. *Carbohydrate Polymers*, *91*(1), 322–332.

Balandin, A. A. (2011). Thermal properties of graphene and nanostructured carbon materials. *Nature Materials*, *10*(8), 569–581.

Castro Neto, A. H., Guinea, F., Peres, N. M. R., Novoselov, K. S., & Geim, A. K. (2009). The electronic properties of graphene. *Reviews of Modern Physics*, *81*(1), 109–162.

Chen, M., Diao, G., & Zhang, E. (2006). Study of inclusion complex of β-cyclodextrin and nitrobenzene. *Chemosphere*, *63*(3), 522–529.

Chen, M., Meng, Y., Zhang, W., Zhou, J., Xie, J., & Diao, G. (2013). β-Cyclodextrin polymer functionalized reduced-graphene oxide: Application for electrochemical determination imidacloprid. *Electrochimica Acta*, *108*, 1–9.

Chen, M., Wang, J., Zhang, W., & Diao, G. (2013). Preparation and characterization water-soluble inclusion complexes of imidacloprid-β-cyclodextrin polymer and their electrochemical behavior. *Journal of Electroanalytical Chemistry*, *696*, 1–8.

Cui, P., Seo, S., Lee, J., Wang, L., Lee, E., Misook Min, M., et al. (2011). Nonvolatile memory device using gold nanoparticles covalently bound to reduced graphene oxide. *ACS Nano*, *5*(9), 6826–6833.

Dong, H., Li, Y., Yu, J., Song, Y., Cai, X., Liu, J., et al. (2013). A versatile multicomponent assembly via β-cyclodextrin host–guest chemistry on graphene for biomedical applications. *Small*, *9*(3), 446–456.

Geim, A. K. (2009). Graphene: Status and prospects. *Science*, *324*(5934), 1530–1534.

Grabar, K. C., Allison, K. J., Baker, B. E., Bright, R. M., Brown, K. R., Freeman, R. G., et al. (1996). Two-dimensional arrays of colloidal gold particles: A flexible approach to macroscopic metal surfaces. *Langmuir*, *12*(10), 2353–2361.

Guo, Y., Guo, S., Li, J., Wang, E., & Dong, S. (2011). Cyclodextrin–graphene hybrid nanosheets as enhanced sensing platform for ultrasensitive determination of carbendazim. *Talanta*, *84*(1), 60–64.

Guo, Y., Guo, S., Ren, J., Zhai, Y., Dong, S., & Wang, E. (2010). Cyclodextrin functionalized graphene nanosheets with high supramolecular recognition capability: Synthesis and host–guest inclusion for enhanced electrochemical performance. *ACS Nano*, *4*(7), 4001–4010.

Hong, W., Bai, H., Xu, Y., Yao, Z., Gu, Z., & Shi, G. (2010). Preparation of gold nanoparticle/graphene composites with controlled weight contents and their application in biosensors. *The Journal of Physical Chemistry C*, *114*(4), 1822–1826.

Hummers, W. S., & Offeman, R. E. (1958). Preparation of graphitic oxide. *Journal of the American Chemical Society*, *80*(6), 1339.

Jiao, X. X., Luo, H. Q., & Li, N. B. (2013). Fabrication of graphene–gold nanocomposites by electrochemical co-reduction and their electrocatalytic activity toward 4-nitrophenol oxidation. *Journal of Electroanalytical Chemistry*, *691*, 83–89.

Konkena, B., & Vasudevan, S. (2013). Resonance Raman detection and estimation in the aqueous phase using water dispersible cyclodextrin: Reduced-graphene oxide sheets. *Analytical Chemistry*, *85*(10), 5114–5119.

Kou, R., Shao, Y., Mei, D., Nie, Z., Wang, D., Wang, C., et al. (2011). Stabilization of electrocatalytic metal nanoparticles at metal–metal oxide–graphene triple junction points. *Journal of the American Chemical Society*, *133*(8), 2541–2547.

Liu, F., Choi, J. Y., & Seo, T. S. (2010). DNA mediated water-dispersible graphene fabrication and gold nanoparticle-graphene hybrid. *Chemical Communications*, *46*(16), 2844–2846.

Liu, J., Fu, S., Yuan, B., Li, Y., & Deng, Z. (2010). Toward a universal "Adhesive Nanosheet" for the assembly of multiple nanoparticles based on a protein-induced reduction/decoration of graphene oxide. *Journal of the American Chemical Society*, *132*(21), 7279–7281.

Liu, Z., Zhang, H., Ma, H., & Hou, S. (2011). Selective determination of *p*-nitrophenol based on its unique voltammetric behavior on nanoporous gold. *Electroanalysis*, *23*(12), 2851–2861.

Lu, D., Lin, S., Wang, L., Shi, X., Wang, C., & Zhang, Y. (2012). Synthesis of cyclodextrin-reduced graphene oxide hybrid nanosheets for sensitivity enhanced electrochemical determination of diethylstilbestrol. *Electrochimica Acta*, *85*, 131–138.

Lv, M., Wang, X., Li, J., Yang, X., Zhang, C., Yang, J., et al. (2013). Cyclodextrin-reduced graphene oxide hybrid nanosheets for the simultaneous determination of lead(II) and cadmium(II) using square wave anodic stripping voltammetry. *Electrochimica Acta*, *108*, 412–420.

Mamba, G., Mbianda, X. Y., & Govender, P. P. (2013). Phosphorylated multiwalled carbon nanotube-cyclodextrin polymer: Synthesis, characterisation and potential application in water purification. *Carbohydrate Polymers*, *98*(1), 470–476.

Ogoshi, T., Ichihara, Y., Yamagishi, T., & Nakamoto, Y. (2010). Supramolecular polymer networks from hybrid between graphene oxide and per-6-amino-β-cyclodextrin. *Chemical Communications*, *46*(33), 6087–6089.

Ren, W., Fang, Y., & Wang, E. (2011). A binary functional substrate for enrichment and ultrasensitive SERS spectroscopic detection of folic acid using graphene oxide/Ag nanoparticle hybrids. *ACS Nano*, *5*(8), 6425–6433.

Shao, Y., Wang, J., Wu, H., Liu, J., Aksay, I. A., & Lin, Y. (2010). Graphene based electrochemical sensors and biosensors: A review. *Electroanalysis*, *22*(10), 1027–1036.

Shen, M., Du, Y., Rong, H., Li, J., & Jiang, L. (2005). Preparation of hydrophobic gold nanoparticles with safe organic solvents by microwave irradiation method. *Colloids and Surfaces A: Physicochemical and Engineering Aspects*, *257–258*, 439–443.

Silva, P. S., Gasparini, B. C., Magosso, H. A., & Spinelli, A. (2014). Gold nanoparticles hosted in a water-soluble silsesquioxane polymer applied as a catalytic material onto an electrochemical sensor for detection of nitrophenol isomers. *Journal of Hazardous Materials*, *273*, 70–77.

Tan, L., Zhou, K.-G., Zhang, Y.-H., Wang, H.-X., Wang, X.-D., Guo, Y.-F., et al. (2010). Nanomolar detection of dopamine in the presence of ascorbic acid at β-cyclodextrin/graphene nanocomposite platform. *Electrochemistry Communications*, *12*(4), 557–560.

Tang, Y., Huang, R., Liu, C., Yang, S., Lu, Z., & Luo, S. (2013). Electrochemical detection of 4-nitrophenol based on a glassy carbon electrode modified with a reduced graphene oxide/Au nanoparticle composite. *Analytical Methods*, *5*(20), 5508–5514.

Wang, Y., Shi, Z., Huang, Y., Ma, Y., Wang, C., Chen, M., et al. (2009). Supercapacitor devices based on graphene materials. *The Journal of Physical Chemistry C*, *113*(30), 13103–13107.

Wang, Y., Zhang, S., Du, D., Shao, Y., Li, Z., Wang, J., et al. (2011). Self assembly of acetylcholinesterase on a gold nanoparticles–graphene nanosheet hybrid for organophosphate pesticide detection using polyelectrolyte as a linker. *Journal of Materials Chemistry*, *21*(14), 5319–5325.

Yang, Y., Zhang, Y.-M., Chen, Y., Zhao, D., Chen, J.-T., & Liu, Y. (2012). Construction of a graphene oxide based noncovalent multiple nanosupramolecular assembly as a scaffold for drug delivery. *Chemistry—A European Journal*, *18*(14), 4208–4215.

Yee, C. K., Jordan, R., Ulman, A., White, H., King, A., Rafailovich, M., et al. (1999). Novel one-phase synthesis of thiol-functionalized gold. Palladium, and iridium nanoparticles using superhydride. *Langmuir*, *15*(10), 3486–3491.

Zhang, W., Chen, M., & Diao, G. (2011). Preparation and electrochemical behavior of water-soluble inclusion complex of ferrocene with β-cyclodextrin polymer. *Electrochimica Acta*, *56*(14), 5129–5136.

Zhang, W., Chen, M., Gong, X., & Diao, G. (2013). Universal water-soluble cyclodextrin polymer–carbon nanomaterials with supramolecular recognition. *Carbon*, *61*, 154–163.

Zhang, W., Gong, X., Cai, Y., Zhang, C., Yu, X., Fan, J., et al. (2013). Investigation of water-soluble inclusion complex of hypericin with β-cyclodextrin polymer. *Carbohydrate Polymers*, *95*(1), 366–370.

Zhang, Z., Gu, S., Ding, Y., Shen, M., & Jiang, L. (2014). Mild and novel electrochemical preparation of β-cyclodextrin/graphene nanocomposite film for super-sensitive sensing of quercetin. *Biosensors and Bioelectronics*, *57*, 239–244.

Zhou, J., Chen, M., & Diao, G. (2013). Assembling gold and platinum nanoparticles on resorcinarene modified graphene and their electrochemical applications. *Journal of Materials Chemistry A*, *1*(6), 2278–2285.

Zhou, J., Chen, M., Xie, J., & Diao, G. (2013). Synergistically enhanced electrochemical response of host–guest recognition based on ternary nanocomposites: Reduced graphene oxide-amphiphilic pillar[5]arene-gold nanoparticles. *ACS Applied Materials & Interfaces*, *5*(21), 11218–11224.

Zhu, Y., Murali, S., Cai, W., Li, X., Suk, J. W., Potts, J. R., et al. (2010). Graphene and graphene oxide: Synthesis, properties, and applications. *Advanced Materials*, *22*(35), 3906–3924.

Zu, S.-Z., & Han, B.-H. (2009). Aqueous dispersion of graphene sheets stabilized by pluronic copolymers: Formation of supramolecular hydrogel. *The Journal of Physical Chemistry C*, *113*(31), 13651–13657.